bioRxiv preprint doi: https://doi.org/10.1101/2024.04.04.588123; this version posted April 4, 2024. The copyright holder for this preprint (which was not certified by peer review) is the author/funder, who has granted bioRxiv a license to display the preprint in perpetuity. It is made available under aCC-BY-NC-ND 4.0 International license.

The Structure of the Drp1 Lattice on Membrane

Ruizhi Peng*[,1], Kristy Rochon*[,2], Scott M. Stagg[#,1,3], Jason A. Mears[#,2,4,5]

[1]Institute of Molecular Biophysics, Florida State University, Tallahassee, Florida, USA

[2]Department of Pharmacology, Case Western Reserve University School of Medicine, Cleveland, OH 44106 USA

[3]Department of Biological Sciences, Florida State University, Tallahassee, Florida, USA

[4]Cleveland Center for Membrane and Structural Biology, Case Western Reserve University School of Medicine, Cleveland, OH 44106 USA.

[5]Center for Mitochondrial Diseases, Case Western Reserve University School of Medicine, Cleveland, OH 44106 USA

Correspondence to J.A. Mears at jason.mears@case.edu and S.M. Stagg at to sstagg@fsu.edu

*R. Peng and K. Rochon contributed equally to this work.

[#]J.A. Mears and S.M. Stagg are joint senior authors.

bioRxiv preprint doi: https://doi.org/10.1101/2024.04.04.588123; this version posted April 4, 2024. The copyright holder for this preprint (which was not certified by peer review) is the author/funder, who has granted bioRxiv a license to display the preprint in perpetuity. It is made available under aCC-BY-NC-ND 4.0 International license.

SUMMARY (40 words)

This study provides new insights into the structure of Drp1 on lipid membranes. A locally ordered Drp1 lattice structure is solved and reveals intermolecular contacts and conformational rearrangements that suggest a mechanism for constriction of mitochondrial membranes.

bioRxiv preprint doi: https://doi.org/10.1101/2024.04.04.588123; this version posted April 4, 2024. The copyright holder for this preprint (which was not certified by peer review) is the author/funder, who has granted bioRxiv a license to display the preprint in perpetuity. It is made available under aCC-BY-NC-ND 4.0 International license.

ABSTRACT (160 words)

Mitochondrial health relies on the membrane fission mediated by dynamin-related protein 1 (Drp1). Previous structural studies of Drp1 on remodeled membranes were hampered by heterogeneity, leaving a critical gap in the understanding of the mitochondrial fission mechanism. Here we present a cryo-electron microscopy structure of full-length human Drp1 decorated on membrane tubules. Using the reconstruction of average subtracted tubular regions (RASTR) technique, we report that Drp1 forms a locally ordered lattice along the tubule without global helical symmetry. The filaments in the lattice are similar to dynamin rungs with conserved stalk interactions. Adjacent filaments are connected by GTPase domain interactions in a novel stacked conformation. Additionally, we observed contact between Drp1 and membrane that can be assigned to variable domain sequence. We identified two states of the Drp1 lattice representing conformational changes related to membrane curvature differences. Together these structures revealed a putative mechanism by which Drp1 constricts mitochondria membranes in a stepwise, “ratchet” manner.

bioRxiv preprint doi: https://doi.org/10.1101/2024.04.04.588123; this version posted April 4, 2024. The copyright holder for this preprint (which was not certified by peer review) is the author/funder, who has granted bioRxiv a license to display the preprint in perpetuity. It is made available under aCC-BY-NC-ND 4.0 International license.

INTRODUCTION

Mitochondria constantly undergo fission and fusion to regulate their morphology, distribution, and size. This dynamic equilibrium is pivotal for numerous cellular processes, including apoptosis, cell cycle progression, damage isolation, and the overall maintenance of mitochondrial health (Nunnari and Suomalainen, 2012; Otera et al., 2013; Wasiak et al., 2007). Drp1, an evolutionary conserved cytosolic protein, stands as the primary regulator of mitochondrial fission. Genetic deficiencies or mutations in Drp1 result in pronounced mitochondrial anomalies, which are associated with severe neurodevelopmental delay (Bauer et al., 2023; Nolden et al., 2022; Robertson et al., 2023). Conversely, enhancement of Drp1 activity is implicated in neurodegenerative disorders such as Parkinson's, Alzheimer's, and Huntington's disease (Haun et al., 2013; Wang et al., 2011; Yan et al., 2015).

Mitochondria fission by Drp1 is a multistep process. Previous studies showed that Drp1 is recruited by Mff and MiD49/MiD51 to the outer mitochondrial membrane (OMM) in mammals (Osellame et al., 2016). Then, Drp1 is reported to oligomerize through interactions with membrane lipids forming ring shape structures (Fröhlich et al., 2013; Ingerman et al., 2005). GTP hydrolysis promotes the constriction of the ring structure, providing the contractile force needed to mediate mitochondrial division (Francy et al., 2015; Koirala et al., 2013). While Drp1 plays a central role in mitochondria fission, the conformational changes required to drive the assembly and constriction of this contractile machinery are poorly understood.

Mechanistic understanding of Drp1 is largely inferred from dynamin superfamily proteins (DSPs), which have been extensively studied by structural biologists. Crystallographic studies showed that Drp1 has similar domain arrangement when compared with dynamin, including a highly conserved GTPase domain (G domain), connected by a bundle-signaling element (BSE) to stalk region, composed of coiled-coil sequence formed by the middle domain and GTPase effector domain (GED). Dynamin has been reported to form a helical lattice along membrane tubules, and great efforts have been made to reconstruct dynamin remodeled membrane structures using helical symmetry (Chappie et al., 2011; Kong et al., 2018; Sundborger et al., 2014; Zhang and Hinshaw, 2001). Recently, a high resolution cryo-electron microscopy (cryo-EM) structure of dynamin1 helices using helical symmetry reconstruction revealed the molecular mechanism of dynamin helix formation and how these structures channel the energy of GTP hydrolysis to constrict membranes through a compression of helical symmetry (Kong et al., 2018). However, similar studies with mitochondrial fission DSPs show an expansion of helical lattices upon GTP hydrolysis (Mears et al., 2011). This suggests that the constriction mechanism may be different for Drp1, which is likely due to the larger magnitude of constriction for these oligomers that encircle intact mitochondria. These larger, dynamic lattice structures of Drp1 remodel membrane into tubules with heterogeneous diameters. When incubated with liposomes *in vitro*, Drp1 can form helical lattices with diameters ranging from 50 - 150 nm (Francy et al., 2017; Fröhlich et al., 2013; Kalia et al., 2018; Macdonald et al., 2014) making it suboptimal candidate for helical symmetry reconstruction. Earlier, a cryo-EM study showed that Drp1 forms linear co-filament with MiD49, where Drp1 elongated via interfaces in the central stalk region similar to interactions observed in dynamin 1 helices (Kalia et al., 2018). However, the molecular mechanism of Drp1 forming circular rings on lipid membranes is still

bioRxiv preprint doi: https://doi.org/10.1101/2024.04.04.588123; this version posted April 4, 2024. The copyright holder for this preprint (which was not certified by peer review) is the author/funder, who has granted bioRxiv a license to display the preprint in perpetuity. It is made available under aCC-BY-NC-ND 4.0 International license.

under investigation. And commonly used helical symmetry reconstruction methods struggle to overcome the challenge of heterogeneity in Drp1 (Francy et al., 2017).

We previously developed a technique called reconstruction of average subtracted tubular regions (RASTR) to handle the challenges of heterogeneity in tubular samples (Randolph and Stagg, 2020). Unlike helical symmetry reconstruction, which requires the protein lattice to be globally ordered, RASTR aims to break down the whole lattice into individual surfaces and capture the locally ordered sections. Instead of reconstructing whole tubular segments, individual tubular surfaces are upweighted and extracted. The resulting sub-particles are refined without imposing symmetry allowing for resolution of regions of the structure that deviate from helical symmetry. We previously showed that RASTR can reconstruct tubular filaments with similar resolution and detail as with helical reconstruction. Here, we have applied RASTR on membrane tubules decorated with Drp1 that are highly heterogeneous. This resulted in a reconstruction with high-quality features that could be unambiguously assigned to Drp1 domains and secondary structures, which allowed us to build an atomic model of the Drp1 lattice. These results were not possible using traditional helical symmetry reconstruction techniques.

Our reconstructions of Drp1-decorated membrane tubules revealed several novel features. First, we showed that the Drp1 lattice exhibits only local order along the membrane tubule as opposed to long-range order required for helical reconstruction. Secondly, we reconstructed maps representing two states of the Drp1 lattice, which we termed the "stacked state" and the "relaxed state". In both maps, discernible stalk features were present, consistent with previous knowledge that DSPs elongated via stalk interfaces (Kalia et al., 2018; Kong et al., 2018). In the stacked state map, we identified a novel organization within the dimer pair that exhibits alternating extended and contracted G domain conformations. These different orientations allow G domains to stack atop one another at different radial locations. Stacked G domains connect Drp1 lattice filaments and hold adjacent rungs close and stable. In the relaxed state, opposing filaments in the lattice were more spaced, accommodating transient G domain contacts that would permit conformational rearrangements and facilitate sliding of adjacent filaments to promote constriction. Examination of the cryo-EM map also revealed a continuous density extending from the body of the protein lattice to the membrane in the stacked state, which highlights lipid interactions with the initial sequence of the Drp1 variable domain (VD). In the relaxed state, this interaction was not observed, consistent with the need to be unanchored at the membrane surface as the filaments constrict. Altogether, our cryo-EM structure provided new insight into Drp1 remodeled membrane tubules and suggested a model for the mechanism by which Drp1 constricts the diameter of mitochondria.

bioRxiv preprint doi: https://doi.org/10.1101/2024.04.04.588123; this version posted April 4, 2024. The copyright holder for this preprint (which was not certified by peer review) is the author/funder, who has granted bioRxiv a license to display the preprint in perpetuity. It is made available under aCC-BY-NC-ND 4.0 International license.

RESULTS

Drp1 is locally ordered on GalCer tubes.

DSPs have been shown to remodel liposomes into tubules *in vitro* (Sweitzer and Hinshaw, 1998; Zhang and Hinshaw, 2001). Electron microscopy studies showed that dynamins form an ordered helical protein lattice on membrane tubules. Given the success of the iterative helical real space reconstruction approach (Egelman, 2007), we and other researchers have successfully used helical symmetry reconstruction to resolve the structure of DSPs (Alvarez et al., 2017; Francy et al., 2017; Kalia et al., 2018; Kong et al., 2018; Sundborger et al., 2014). However, structure determination of Drp1-decorated membranes has been impeded by sample heterogeneity. It was demonstrated that upon incubation of Drp1 with liposomes, protein-decorated tubules were formed, but these tubules exhibited significant variability in their diameters, complicating the application of helical reconstructions (Francy et al., 2015; Fröhlich et al., 2013; Kalia et al., 2018; Macdonald et al., 2016). To mitigate this sample heterogeneity, we employed galactosyl ceramide lipids (GalCer) as a substrate (Wilson-Kubalek et al., 1998). GalCer lipids inherently form membrane nanotubes with a consistent diameter of approximately 20 nm (inner lumen), thereby constraining the diameter of Drp1-remodeled membranes. We incubated full-length Drp1 isoform 3 with negatively charged GalCer tubes in the presence of 1 mM GMPPCP. Upon incubation with GalCer tubes, well-defined protein decorations were observed (Fig. S1A). However, layer lines with features able to be indexed were still not observed in the Fourier transforms of the tubules (Fig. S1, B & C). Consequently, we hypothesized that the lattice structures formed by Drp1 exhibit only local order, lacking long-range organizational coherence.

To validate this hypothesis and determine the size of the locally ordered area, we employed the RASTR technique (Randolph and Stagg, 2020) on the cryo-EM dataset of Drp1-coated tubules. Particles were first processed using RASTR with four distinct spherical mask radii, all oriented on the middle of the tubule. As the mask diameter was reduced, a progressively smaller region of interest (ROI) was extracted from the original particles. These particle stacks were then independently aligned and classified in two dimensions (Fig. 1A). The largest ROI mask produced a 2D average with diffuse continuous stripes of density like a barber pole going up the tubule axis. With a smaller 250 Å ROI mask, individual puncta were observed breaking up the continuous stripes of density in the middle of the tubules. With ROI masks smaller than 185 Å, more details were observed such as individual stalk regions and adjacent G-domains. These findings corroborated the notion that

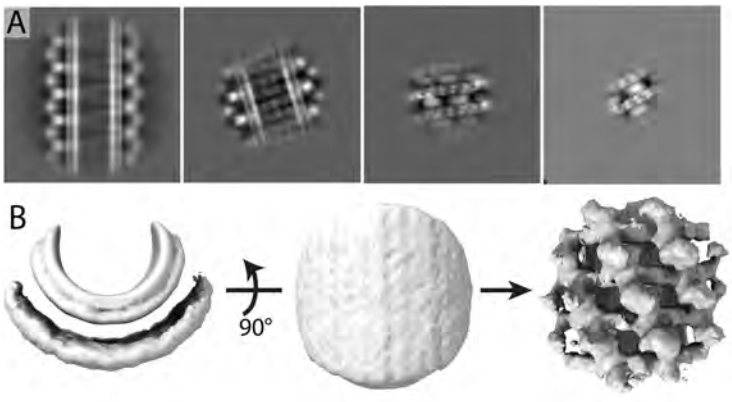

Figure 1. Drp1 lattice on GalCer tubes exhibit local order. (A) 2D classification of Drp1 particles with four different radii of ROI. From left to right, 425 Å, 250 Å, 185 Å, 130 Å. Box size, 888 Å. **(B)** Data processing for getting initial model. Left and middle, masked azimuthal average map. Right, Best 3D class map.

bioRxiv preprint doi: https://doi.org/10.1101/2024.04.04.588123; this version posted April 4, 2024. The copyright holder for this preprint (which was not certified by peer review) is the author/funder, who has granted bioRxiv a license to display the preprint in perpetuity. It is made available under aCC-BY-NC-ND 4.0 International license.

Drp1 lattice was only locally ordered on GalCer tubes. This analysis revealed why the full tubule particles were suboptimal candidates for helical symmetry reconstruction; however, when processed via RASTR using a mask radius that aligned with the area of local order, they exhibited well-aligned, high-resolution features.

After selecting an appropriate ROI, we set about determining the 3D structure of the locally ordered Drp1 lattice. First, we needed an initial model for the single particle refinement without high-resolution features that might align spuriously to noise in the images, and the azimuthal average from the RASTR process provided a good initial model. Briefly, the azimuthal average was created by applying shifts and angle rotations to each particle image, making the tube axis at the center of the image and parallel to z axis. Images were rotated randomly around the tube axis, yielding the azimuthal average map (Fig. 1B, left two panels). For Drp1, the azimuthal average map contained no high-resolution protein features but rather concentric layers of densities representing the two lipid bilayer leaflets and a smeared-out protein layer. After the azimuthal average initial model was made, we conducted 3D classification with eight classes using C1 symmetry in RELION. One class converged to a coherent structure, displaying distinct domain features (Fig. 1B, far right density). These features, representing G domain and stalk structures, exhibited repeats at fixed angle twist and vertical rise, consistent with the canonical structural pattern observed in other DSPs (Kong et al., 2018; Liu et al., 2021). The fact that no symmetry was applied during refinement and that the initial model was featureless, providing no bias, demonstrated that the result was completely data driven. Based on this map, we estimated the helical symmetry parameters for the full helical filament. When we attempted a single particle reconstruction on full tubules with these parameters, the densities became smeared due to averaging of non-uniform features (Fig. S1D), further demonstrating that Drp1 exhibits only local order when decorating GalCer tubes.

Structure of the Drp1 Lattice on GalCer tubules.

The resolution of the Drp1 map was improved with further local Euler angle refinement in *cis*TEM (Fig. S2). This resulted in a map at 11.37 Å resolution (Fig. 2B, Fig. S2B) that elucidated the features of the Drp1 lattice to a degree that enabled the construction of unambiguous atomic models (Fig. 2C).

The Drp1 map showed features that were consistent with other DSPs. Specifically, a continuous filament was built via conserved intermolecular interfaces (numbered 1-3) between stalks (Kalia et al., 2018; Kong et al., 2018; Liu et al., 2021; Reubold et al., 2015). In our map, the best resolved region represented the stalk filament (Fig. 2, purple), which connects the peripheral BSE to the membrane proximal VD (red and brown, respectively; Fig. S3A, Fig. S3B). This elongated structure coordinated intermolecular contacts via the same interfaces (Interfaces 1-3, Fig. S3C) previously reported (Kalia et al., 2018; Kong et al., 2018). In this way, the lattice builds through conserved interactions at well-defined interfaces. Conversely, differences in inter-domain organization were found in the BSE and G domain densities.

bioRxiv preprint doi: https://doi.org/10.1101/2024.04.04.588123; this version posted April 4, 2024. The copyright holder for this preprint (which was not certified by peer review) is the author/funder, who has granted bioRxiv a license to display the preprint in perpetuity. It is made available under aCC-BY-NC-ND 4.0 International license.

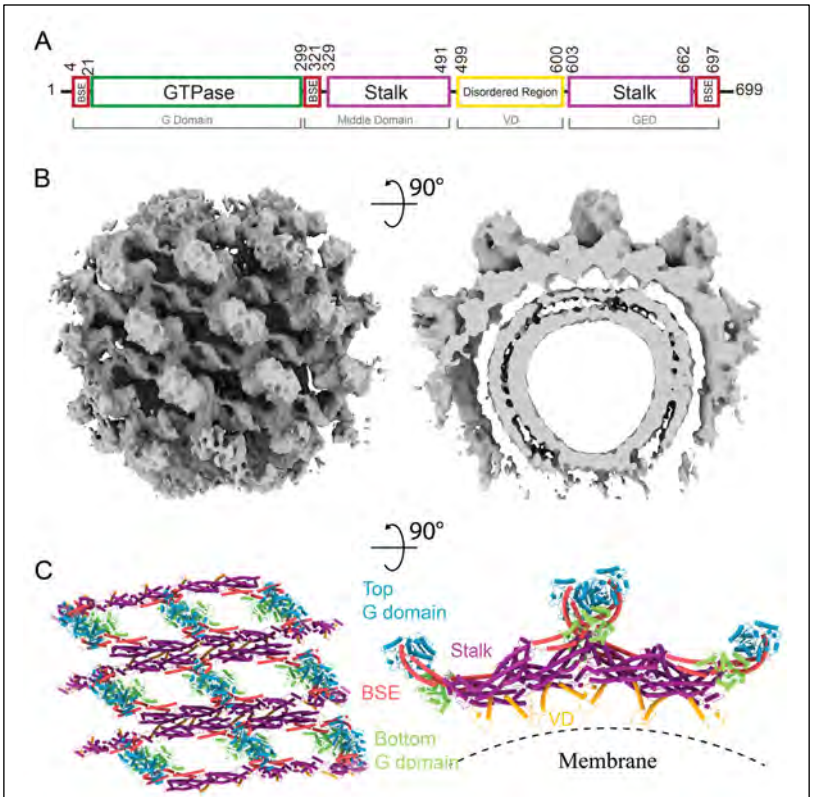

Figure 2. Architecture of assembled Drp1 in the GMPPCP-bound state on GalCer tubes. (A) Domain arrangement of Drp1. **(B)** Cryo-EM map of Drp1 decorated GalCer tubes. Image on the right is sliced to show one rung. **(C)** Lattice models built (two tetramer shown). Image on the right is showing two tetramers. Purple, stalk domain; Red, BSE; Green, bottom G domain; Blue, top G domain; Brown, VD domain.

Given that the domains and features of Drp1 proteins in the lattice could be unambiguously identified, atomic models were built by fitting previously determined Drp1 structures and domains into the cryo-EM density. Initially, we tried to fit solely the extended conformation dimer (Kalia et al., 2018) (RCSB: 5WP9) or the contracted conformation dimer (Fröhlich et al., 2013) (RCSB: 4BEJ); however, half of the globular densities attributable to the G domains were unoccupied because one G domain in the dimer pair could not fit in those configurations. Therefore, we employed a strategy of fitting two states of dimers in the map. Using rigid body docking, the crystal structure (RCSB: 4BEJ) stalks aligned with minimal effort; however, it was clear the bottom G domains (Fig. 3, A & B) in the lattice would require a conformation where BSE stretched further than that observed in the crystal structure. The cryo-EM filament structure (RCSB: 5WP9) has an extended G domain conformation and was able to fit within the stalk density while still spanning the distance needed to reach the interface of the bottom G domains. Isolating the density representing the smallest asymmetric subunit of the lattice by removing the rest of the map, a combination of two crystal structure monomers and two filament structure monomers were fit into the map (Fig. 3A). The interface aligning the four G domain monomers was positioned based on the structure of the dynamin 1 GTPase-GED (GG) fusion protein (Chappie et al., 2011) (RCSB: 3ZYC). This GMPPCP-bound dimer formed through G domain contacts that ensured a reasonable starting position comprised of conserved contacts. Once the asymmetric tetramer was fit to the best starting position, it was docked into the full map and additional monomers were added to build the stalk interfaces needed to constrain each monomer within the density. After minimization, Molecular Dynamics Flexible Fit (MDFF) was used to further refine the final asymmetric subunit.

bioRxiv preprint doi: https://doi.org/10.1101/2024.04.04.588123; this version posted April 4, 2024. The copyright holder for this preprint (which was not certified by peer review) is the author/funder, who has granted bioRxiv a license to display the preprint in perpetuity. It is made available under aCC-BY-NC-ND 4.0 International license.

Surprisingly, the model converged to a configuration featuring two dimers stacked atop one another (Supplementary Video 1, Fig. 3, A & B). Previous studies typically showed Drp1 dimers to be either in an apo state or a GTP-bound state, with both G domains exhibiting the same conformation (Fröhlich et al., 2013; Kalia et al., 2018). However, in our model, each dimer possessed G domains in two distinct states, with one G domain position achieved through an extended conformation and the partner G domain in a contracted conformation (Fig. 3, B & C). This was consistent with a recent in-solution structure that showed that the hinge 1 loop in Drp1 is flexible, so the relative positions of the BSE and stalks are not restricted (Rochon et al., 2024). Within the context of this tetrameric model, the interfaces between stalks remained consistent (Fig. S3C). Another difference was the interface between G domains. In our model, the GG interface between the bottom G domains is the same as dynamin 1 (Fig. S3D, green). The top GG interface is similar, but there is a ~10 Å shift (Fig. S3D, blue) compared to the bottom interfaces or dynamin.

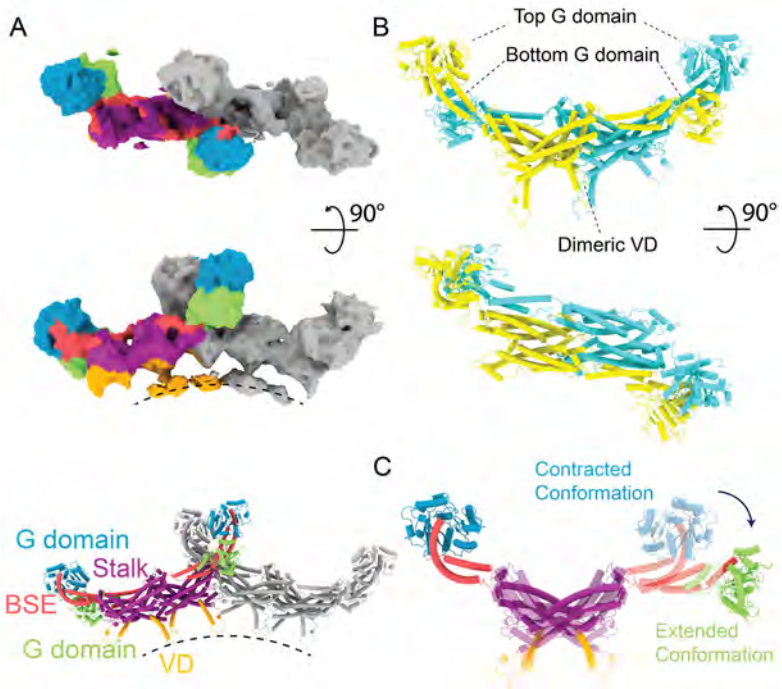

Figure 3. Asymmetric tetramer. (A) Segmented Cryo-EM map and models showing two tetramers within same rung. One colored, another gray. **(B)** Asymmetric tetramer. Yellow and cyan representing two dimers. **(C)** Conformational change induced by nucleotide binding. Purple, stalk domain; Red, BSE; Green, bottom G domain in extended conformation; Blue, top G domain in contracted conformation; Brown, VD domain.

Altogether, the Drp1 lattice structure was characterized by parallel rungs, each of which was elongated through oligomerization of the stalk domains in the same manner as reported before (Kalia et al., 2018). Interposed between these rungs, G domains served as contact sites that stabilized adjacent rungs (Fig. 2C). The smallest repeating subunit was a tetramer, with two dimers stacking atop one another (termed the “stacked state”). Individual dimer in our structures was asymmetric, with one G domain in extended conformation and the other G domain in a contracted conformation.

G domain conformational change in Drp1 lattice

In another dataset, Drp1 decorated GalCer tubes were formed with 2 mM GMPPCP, and a surprising discovery was made: an alternative state of the Drp1 lattice was identified, which we termed the "relaxed state" (Fig. 4A, right). At the vertical center of this map, densities corresponding to stalks were observed, indicating the stable intermolecular interactions

bioRxiv preprint doi: https://doi.org/10.1101/2024.04.04.588123; this version posted April 4, 2024. The copyright holder for this preprint (which was not certified by peer review) is the author/funder, who has granted bioRxiv a license to display the preprint in perpetuity. It is made available under aCC-BY-NC-ND 4.0 International license.

between stalks. However, the stacked G domain densities were absent in this relaxed state lattice (Fig. 4B). Instead, a diffuse cloud of densities appeared at the radial position corresponding to the bottom G domains, while densities at the radial position of the top (i.e. most peripheral) G domains were not observed. In the relaxed state of the Drp1 lattice, the central rung corresponding to stalk densities was consistent with the stacked state map, but stalk densities in adjacent rungs were less well-defined (Fig. 4A). Additionally, we noted a curvature change between these two states. In the stacked state, the lipid membrane curvature exhibited local flattening at the center of the target region. But in the relaxed state, the curvature at the center was higher (Fig. 4C). We didn't attempt to build a complete model on this map because of the diffuse and incoherent densities observed for the G domain cloud and adjacent rungs. However, it was clear that the stalk domain organization and interfaces were conserved between the two structures, but the G domains largely adopted the extended conformation and were not well defined either due to heterogeneity or changes to the BSE extension. Importantly, the change of G domain conformation correlated with the curvature change.

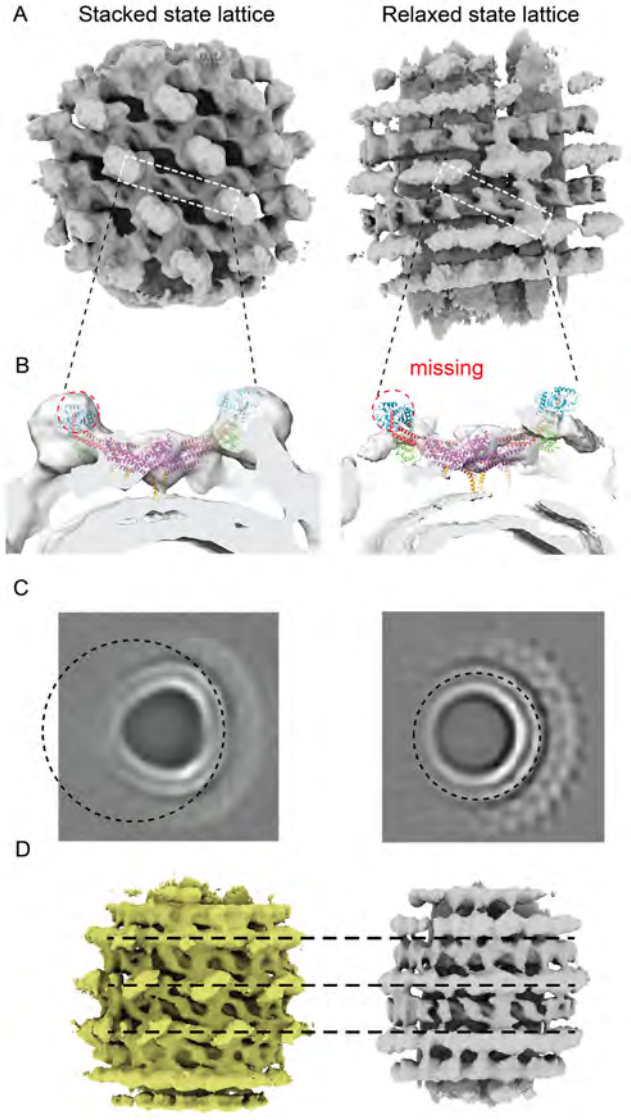

Figure 4. Comparison of Drp1 lattice in two states. (A) Cryo-EM map of Drp1 lattice. **(B)** Focused view showing one tetramer. Density of top G domain is missing in extended state map. **(C)** Projection of Cryo-EM map along tube axis. Local flattening of membrane densities in stacked state map. Left showing stacked state, right showing extended state. Purple, stalk; Red, BSE; Green, bottom G domain; Blue, top G domain; Brown, VD domain. **(D)** Side-by-side comparison of spacing between Drp1 lattice rungs. Maps are from two end of PC1 axis in cryoDRGN latent space. Maps are rotated so that Drp1 rungs are horizontal.

Previous investigations into Drp1 proteins recognized the fission process as a continuous, dynamic process, with the diameter of Drp1 rings gradually decreasing. In the two states that we captured, two distinct curvatures demonstrated the inherent flexibility and dynamic nature of the lattice, potentially representing two intermediate states in the dynamic process. We further investigated the dataset using cryoDRGN, a machine learning based

bioRxiv preprint doi: https://doi.org/10.1101/2024.04.04.588123; this version posted April 4, 2024. The copyright holder for this preprint (which was not certified by peer review) is the author/funder, who has granted bioRxiv a license to display the preprint in perpetuity. It is made available under aCC-BY-NC-ND 4.0 International license.

algorithm for reconstruction of heterogeneous cryo-EM structures (Zhong et al., 2021). In the second dataset, we identified continuous motion in the Drp1 structure. Although the relaxed state lattice structure occupied most of the particles, the stacked state lattice was also present in the dataset. Analyzing the PC1 axis of the cryoDRGN latent space revealed a shift from stacked state lattice to relaxed state lattice (Fig. 4D, Supplementary Video 2). There is a strong correlation between the densities of the top G domains and the spacing of the rungs (Fig. 4D, Supplementary Video 2). When the top G domain density reached its highest occupancy, the spacing between Drp1 rungs was at its shortest, consistent with the stacked state lattice with well-defined G domain pairing. Conversely, at its lowest occupancy, the rung spacing expanded, indicative of the relaxed state lattice. Furthermore, when the top G domain was present, adjacent rungs exhibited similar resolution features. However, in its absence, only the central rung had recognizable stalk features, while adjacent rungs appeared less ordered. Collectively, these findings suggest that the binding of G domains served to stabilize the entire lattice, maintaining the integrity of adjacent rungs. Conversely, compromised G domain binding weakened the connections between adjacent Drp1 lattice rungs, leaving the lattice flexible.

Drp1 lattice contact lipids membrane

A novel feature in our stacked state cryo-EM map was the contact between the Drp1 protein lattice and lipid membranes (Fig. 5A). In traditional helical symmetry reconstructions, such features were often poorly resolved, but the RASTR technique successfully captured them. The contact sites were distributed periodically on the lattice (Fig. 5A), with each membrane contact coinciding with an individual tetramer. Further inspection revealed that these contact sites are located exactly under the proximal tips of the central stalk within tetramers, where the VD sequence starts (VD at center of tetramer) (Fig. 3B, Fig. 5A blue, Fig. 5B top). We observed extended densities in the region of the stalk tips between tetramers (VD at junctions between tetramers), but these were of much lower occupancy and contact with lipid membrane densities was not observed (Fig. 5A). Tracing back from the VD to monomers, we discovered that the VD structures at the center all originated from monomers with G domains in a contracted conformation, whereas weaker VD interactions at intervening junctions all originated from monomers with G domains in an extended conformation (Fig. 5B). The different occupancies of the contact densities indicated a strong relationship between VD-lipid interactions and G domain conformation (Fig. 5B). In support of this, we didn't observe membrane contact in the relaxed state lattice (Fig. 4B), where no G domains were in contracted conformation. Together, the membrane interactions correlated with G domain conformations in a pattern where stronger G domain interactions (tight rung spacing) favored membrane connections and relaxed G domain contacts weakened this connection, which would permit lattice rearrangements (i.e. constriction).

The Drp1 VD is 102 amino acids long and has been attributed to have a regulatory function by interacting with lipids (Adachi et al., 2018; Adachi et al., 2016; Francy et al., 2015; Ugarte-Uribe et al., 2014). Several important charged residues in this region are associated with specificity for negatively charged lipid headgroups (Mahajan et al., 2021). However, the VD was either truncated or not resolved in previous structure studies (Fröhlich et al., 2013; Kalia et al., 2018). Because the protein lattice interacts in a regular pattern in the stacked state map, we reasoned

bioRxiv preprint doi: https://doi.org/10.1101/2024.04.04.588123; this version posted April 4, 2024. The copyright holder for this preprint (which was not certified by peer review) is the author/funder, who has granted bioRxiv a license to display the preprint in perpetuity. It is made available under aCC-BY-NC-ND 4.0 International license.

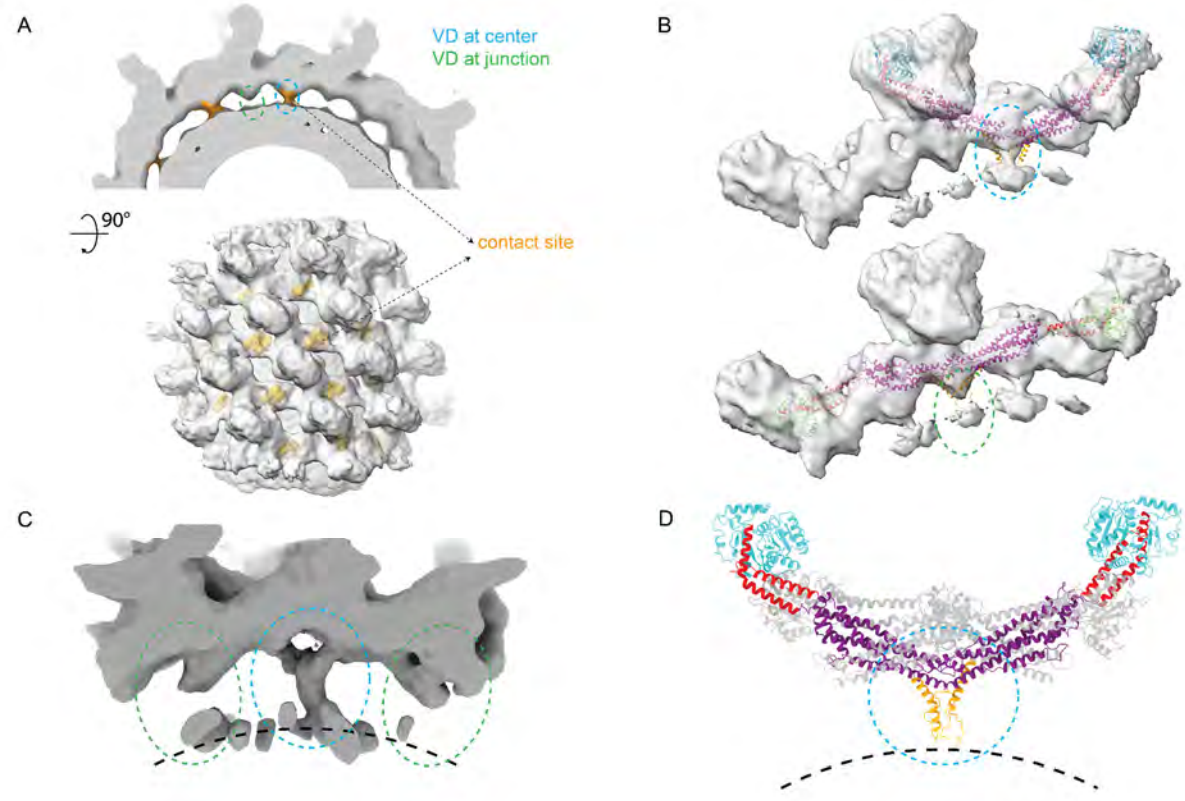

Figure 5. Contact between Drp1 lattice and lipids membrane. **(A)** Cryo-EM map slice showing contact between Drp1 lattice density with lipids membrane density. Contact density colored by brown. Green dash circle indicating VD position of bottom G domain containing Drp1 monomer. Cyan dash circle indicate VD position of top G domain containing Drp1 monomer. **(B)** Focused view showing differences in membrane contact densities. Map are segmented from Fig. 2A. Left, membrane contact within tetramers. Right, membrane contact between tetramers. **(C)** Cryo-EM map of sub-particle reconstruction at contact position. **(D)** Focused view of VD domain model. Monomer with top G domain conformation is colored. Monomer with bottom G domain conformation is colored gray.

that the density for the VD may be apparent at lower resolution when compared to the rest of the map. Therefore, a sub-particle reconstruction strategy was employed to refine the VD proximal to the membrane, specifically focusing on the region within a tetramer. In the resulting reconstruction, we observed densities extending from the terminal of the two paired stalks (Fig. 5C). These densities extended towards membrane and fuse together forming a thicker rod-like density (Supplementary Video 3). Notably, despite not enforcing symmetry during the refinement process, the resulting map showed a C2-symmetric density that was consistent with a pair of helices contributed by adjacent VDs.

The N-terminal end of the VD, which has been termed the Molecular Recognition Feature 1 (MoRF-1)(Mahajan et al., 2021) has been predicted to be helical. This helix at residues 499-520 was also predicted by AlphaFold (Jumper et al., 2021). MoRFs were found in Intrinsically Disordered Regions (IDRs) and were capable of transitioning from a disordered to ordered under favorable conditions, like partner protein binding (Bugge et al., 2020; Fung et al., 2018). There were no published structures of Drp1 with a resolved density for VD. Based on the sub-

bioRxiv preprint doi: https://doi.org/10.1101/2024.04.04.588123; this version posted April 4, 2024. The copyright holder for this preprint (which was not certified by peer review) is the author/funder, who has granted bioRxiv a license to display the preprint in perpetuity. It is made available under aCC-BY-NC-ND 4.0 International license.

particle reconstruction map, we docked the MoRF-1 helix into this contact position, forming an interface between the two adjacent helices in neighboring Drp1 monomers (Fig. 5D). These coupled helices formed a local dimeric conformation that reached down to touch the surface of the lipid bilayer (Fig. 5D).

DISCUSSION

Here, we reconstructed the structure of the Drp1 lattice on membrane tubules. Despite the inherent flexibility of Drp1 particles, which renders them unsuitable for helical symmetric reconstruction, we demonstrated that localized order exists within the particles that can be extracted using RASTR and subsequently reconstructed. This approach revealed to novel features about membrane bound Drp1 structure, including the discovery of stacked and relaxed states of the lattice, the development of a novel model featuring an asymmetric tetramer as the repeating subunit, and the observation of membrane contacts in the VD that occur in alternating Drp1 dimers in the stacked state.

Previous research on analogous membrane remodeling proteins has predominantly employed helical symmetry reconstruction (Kalia et al., 2018; Kong et al., 2018; Nguyen et al., 2020; Zhang and Hinshaw, 2001). However, this approach necessitates the protein lattice to exhibit long-range order. Many membrane remodeling proteins are only locally ordered in reflection of the heterogeneous and flexible nature of membranes (Kong et al., 2018; von der Malsburg et al., 2023). Consequently, cryo-EM reconstructions lack high-resolution features and/or have ambiguous lattice order. Our current study underscores the potential of RASTR in addressing these challenges. By focusing on the ordered surfaces of the protein lattices, RASTR enables the extraction of structural features from Drp1 that were not resolved using conventional helical processing. The Drp1 lattice determined by RASTR clearly exhibited parallel rungs indicative of the stalk densities, complemented by globular densities that correspond to the GTPase domains. With this insight, pseudoatomic models were developed to inform structural mechanisms of the protein assembly and subsequent constriction.

First, the structure of Drp1 decorated membrane tubules was resolved with the Drp1 G domains in a novel stacked state, built through complementary interactions asymmetric tetramers. This tetramer model was comprised of two identical dimers: one half with G domains in a contracted conformation and the other half in an extended conformation. The two conformations differ in the BSE and hinge 1 regions, leading to an extended BSE hinge. To span the distance needed in the extended state lattice, the BSE hinge swings outward, similar to the position observed in the filament structure of Drp1 paired with MiD49 (Kalia et al., 2018) and a truncated dynamin nucleotide-bound structure (Chappie et al., 2011). This structure also highlights the ability of hinge 1 to confer large conformational rearrangements of the G domain while still maintaining ordered stalk interfaces.

The stacked state for the G domains has not been observed previously in Drp1 reconstructions in the absence of membrane, nor has a similar state been observed in other DSPs. There are many supporting pieces of evidence that support these results. First, the Drp1 lattice was resolved in the reconstruction after starting with the featureless azimuthal average as the initial model for refinement. No symmetry was imposed during refinement yet nearly identical

bioRxiv preprint doi: https://doi.org/10.1101/2024.04.04.588123; this version posted April 4, 2024. The copyright holder for this preprint (which was not certified by peer review) is the author/funder, who has granted bioRxiv a license to display the preprint in perpetuity. It is made available under aCC-BY-NC-ND 4.0 International license.

features were resolved for the different asymmetric units in the resulting lattice. In this way, the map is self-validating. Another strong supporting piece of data is that the stacked state was recapitulated when classifying a second dataset (2 mM GMPPCP) that exhibited a greater degree of heterogeneity. This revealed that the Drp1 lattice undergoes a breathing motion with continuous flexibility from a relaxed state where only one set of G domains in the Drp1 asymmetric tetramer are well-ordered to a compacted stacked state, where both sets of G domains are ordered and are stacked on top of one another. Together, these G domain interactions in the Drp1 lattice are more dynamic when compared to dynamin structures. In the dynamin structure (Kong et al., 2018), the G domain pairing is continuous and uniform. In the Drp1 lattice, the variation in inter-rung distance coincides with the altered pairing between adjacent G-domains. In the relaxed state, only one of the G domain pairs is observed, suggesting that the other domains are unpaired, or irregular. This would be consistent with the weaker interactions between rungs that lead to variability in spacing. This G domain pairing is critical for the stimulated activity of DSPs on lipid membranes, and consistent with previous biochemical findings, the stimulation of Drp1 GTPase activity is much lower than that observed with dynamin (~10-15-fold stimulation for Drp1 compared to ~100-fold stimulation for dynamin)(Bustillo-Zabalbeitia et al., 2014; Chappie et al., 2010; Macdonald et al., 2014; Warnock et al., 1996).

Having resolved the two states of the Drp1 lattice, we are now better positioned to elucidate the pronounced heterogeneity exhibited by Drp1 when incubated with lipid membranes. In the relaxed state of the Drp1 map, it's evident that adjacent rung densities become diffused, suggesting that they are excessively flexible. Conversely, in the stacked state lattice, overall contacts between G domains are stronger, ensuring adjacent rungs are held firmly and closely. Interestingly, adjacent rungs in stacked state lattice are held by asymmetric GG contacts, and the top pair is lost in the relaxed state. Since this top G domain pair is in a contracted conformation, the natural changes that would follow disruption of this pair is extension of the G domain. This directionality is consistent throughout the lattice, and transition between the contracted and extended conformations would drive constriction of the Drp1 lattice as adjacent rungs ratchet through alternating G domain pairing (Supplemental Video 4). Consequently, throughout Drp1 tubules, some regions of the lattice will exhibit a relaxed state, while others will be stacked.

Our RASTR reconstruction of the Drp1 stacked state lattice revealed that the VD becomes ordered and contacts the membrane. We discerned that in the stacked state lattice, the first ~20 residues in the VD occupy a vertical position, extending from the distal end of stalk to the outer leaflet of the membrane. Moreover, we discovered that the VD situated at the center of a tetramer exhibits a pronounced connection with the membrane, whereas the VD located at the junction between adjacent tetramers is sparsely populated (Fig. 5A). This is reminiscent of the asymmetry observed in the dynamin lattice, where the PH domains impinge on the membrane depending on the conformation of the rest of the monomer. A similar phenomenon may be at play in the Drp1 lattice where the state of the G domain interactions is transmitted to the lipid-binding segment of the protein. In the same way that constriction of the lattice requires dynamic G domain interactions, the VD interactions with the membrane are likely dynamic in a

bioRxiv preprint doi: https://doi.org/10.1101/2024.04.04.588123; this version posted April 4, 2024. The copyright holder for this preprint (which was not certified by peer review) is the author/funder, who has granted bioRxiv a license to display the preprint in perpetuity. It is made available under aCC-BY-NC-ND 4.0 International license.

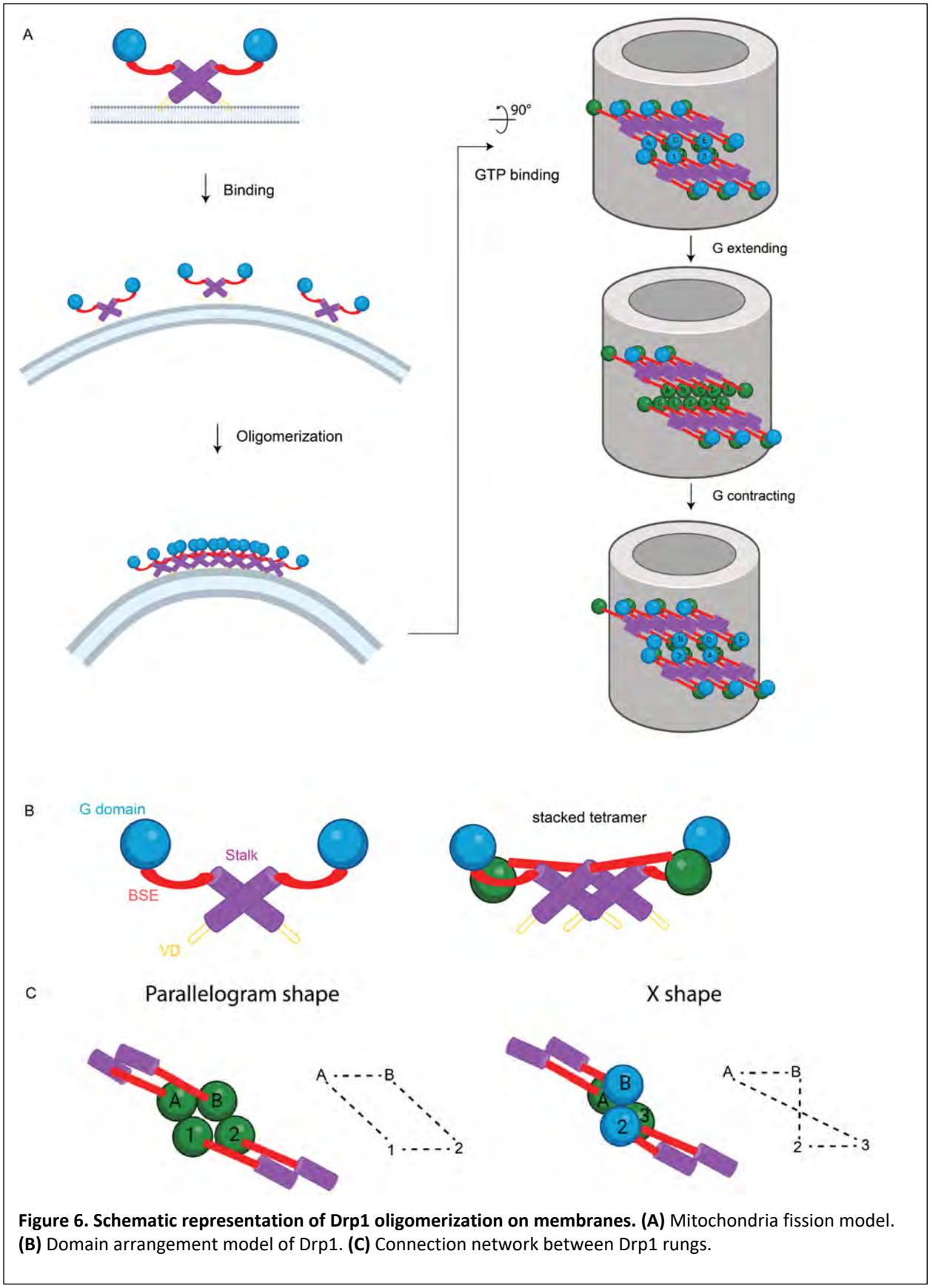

Figure 6. Schematic representation of Drp1 oligomerization on membranes. (A) Mitochondria fission model. **(B)** Domain arrangement model of Drp1. **(C)** Connection network between Drp1 rungs.

bioRxiv preprint doi: https://doi.org/10.1101/2024.04.04.588123; this version posted April 4, 2024. The copyright holder for this preprint (which was not certified by peer review) is the author/funder, who has granted bioRxiv a license to display the preprint in perpetuity. It is made available under aCC-BY-NC-ND 4.0 International license.

coordinated manner that permits sliding on the membrane surface while still maintaining association.

We posit that the cyclical transition of G domain pairing and VD-membrane interactions in transition from the extended state to the relaxed state in Drp1 underpins the sliding and contraction of the Drp1 lattice during mitochondrial remodeling (Fig. 6, Supplementary Video 4). In this model, upon recruitment to the mitochondria, Drp1 proteins extend through interactions at stalk interfaces. As the filament lengthens and encircles the membrane, adjacent rungs connect through the G domain, resulting in a stabilized structure that favors a flatter geometry, which may also explain the preference towards larger tubules with Drp1 when compared with dynamin (100+ nm diameter for Drp1 vs 50 nm for dynamin). The binding of GTP instigates a perpetual transition between the constricted and extended G domain states that facilitate breathing in the lattice from stacked to relaxed states. This conformational flux within the G domain propels the stalk-mediated filaments to slide in the direction of constriction that is biased by the right-handed nature of the lattice and the natural extension of the contracted G domain in the asymmetric dimer that will reach to form a new pair that promotes sliding between rungs and drive the constriction of the lattice. As the lattice approaches higher curvature, the strain on maintaining G domain connections will be greater. In agreement, Drp1 filaments dissociate from the membrane after constriction. It is possible that additional mitochondrial fission factors, including partner proteins and cytoskeletal elements, could stabilize the lattice at higher curvatures to enhance constriction and drive membrane fission.

bioRxiv preprint doi: https://doi.org/10.1101/2024.04.04.588123; this version posted April 4, 2024. The copyright holder for this preprint (which was not certified by peer review) is the author/funder, who has granted bioRxiv a license to display the preprint in perpetuity. It is made available under aCC-BY-NC-ND 4.0 International license.

MATERIALS AND METHODS

Drp1 expression and purification

Drp1 Isoform 3 (UniProt ID O00429-4) was cloned into the pCal-N-EK vector as described previously (Clinton et al., 2020; Clinton et al., 2016). Drp1-3 was expressed in BL21(DE3) Star *Escherichia coli*. Cells were grown in LB containing 100 µg/mL ampicillin at 18 °C with shaking at 200 rpm for 24 hours after induction with 1 mM isopropyl-1-thio-b-D-galactopyranoside (IPTG). Then, cells were harvested via centrifugation at 4,300 × *g* for 20 minutes at 4 °C. The resulting pellet was resuspended in CalA Buffer (0.5 M L-Arginine pH 7.4, 0.3 M NaCl, 5 mM $MgCl_2$, 2 mM $CaCl_2$, 1 mM imidazole, 10 mM β-mercaptoethanol) with 1 mM Pefabloc-SC and 100 mg/mL lysozyme. Cells were lysed by sonication on ice. Next, the cell debris was pelleted via centrifugation at 150,000 × g for 1 hour at 4 °C. First, the CBP-tagged Drp1 was purified by affinity chromatography using calmodulin agarose resin (Agilent) that had been pre-equilibrated with CalA Buffer. After the supernatant was loaded onto the column, the resin was washed with 25 column volumes of CalA Buffer. Next, fractions of eluent were collected using 0.5 column volumes of CalB Buffer (0.5 M L-Arginine pH 7.4, 0.3 M NaCl, 2.5 mM EGTA, 10 mM β-mercaptoethanol). Protein-containing fractions were pooled and incubated with GST-tagged PreScission Protease (HRV-3C) overnight at 4 °C to remove the CBP-tag. This solution was concentrated using a 30,000 molecular weight cut-off centrifugal filter (Amicon). This concentrated pool of Drp1 was further purified by size exclusion chromatography (SEC) with an ÄKTA Purifier FPLC (GE Healthcare) and a HiLoad 16/600 Superdex 200 Prep Grade column that had been pre-equilibrated with SEC Buffer (25 mM HEPES (KOH) pH 7.5, 0.15 M KCl, 5 mM $MgCl_2$, 10 mM β-mercaptoethanol). All elution fractions containing Drp1 were pooled and concentrated once again, and glycerol (5% final) was added. The purified Drp1 was aliquoted, flash frozen in liquid nitrogen, and stored at -80 °C until use.

Generation of Drp1 coated nanotubes

All lipid nanotubes utilized here were comprised of 40% D-galactosyl-beta-1'-N-nervonyl-erythro-sphingosine (GC), 35% phosphatidylethanolamine (PE), and 25% phosphatidic acid (PA). All lipids were purchased from Avanti Polar Lipids, Inc. (Alabaster, AL). Lipids were added to a glass test tube and slowly dried to a thin film using nitrogen gas. The lipid film was then stored in a desiccator for at least one hour to ensure any trace solvent remaining was removed. Then the lipid film was rehydrated with a buffer (200 mL) containing 50 mM HEPES (KOH) pH 7.5 and 0.15 M KCl and heated in 37 °C water bath for ~40 minutes with gentle vortexing every 10 minutes. With these volumes, the final lipid nanotube concentration was 2 mM. The lipid film was placed in a water bath sonicator for 30 seconds and the resulting nanotubes were stored on ice until use. Protein was diluted to 5 µM and incubated at room temperature with lipid nanotubes (500 µM) for at least 30 minutes before adding GMPPCP and 2 mM $MgCl_2$.

Freezing

The sample was frozen using a FEI Vitrobot Mark III. The sample was applied to Holey carbon grids (3.5/1, 400 mesh, Quantifoil) at 4 °C, 100% humidity and incubated on the grid for 60 s. A blot force of 10 and a blot time of 10-12 s was used before plunge freezing into liquid ethane. Samples were stored in liquid nitrogen temperatures before imaging.

bioRxiv preprint doi: https://doi.org/10.1101/2024.04.04.588123; this version posted April 4, 2024. The copyright holder for this preprint (which was not certified by peer review) is the author/funder, who has granted bioRxiv a license to display the preprint in perpetuity. It is made available under aCC-BY-NC-ND 4.0 International license.

Cryo-EM data collection

Drp1 data was collected in two sessions. For the first dataset where Drp1 was incubated with GalCer tubes at 1 mM GMPPCP, data was collected on a Titan Krios (ThermoFisher Scientific). Images were acquired by a DE-64 detector in integrating mode. For the second session where Drp1 is incubated with GalCer tubes at 2 mM GMPPCP, data was collected on the same microscope but with the next generation camera, DE Apollo direct detector (Peng et al., 2023). For both datasets, the microscope was operated at 300 kV with a 50 µm C2 aperture and 100 µm objective aperture. The electron beam in nanoprobe mode was aligned through Direct Alignment in the Titan GUI. Coma-free alignment was performed by acquiring a Zemlin tableau in Leginon (Suloway et al., 2005). Cryo-EM images were acquired using the Leginon software and pre-processed using the Appion package (Lander et al., 2009). Apollo camera was set in 8k × 8k super-resolution mode. Movies were collected at a magnification of 47000× with the pixel size of 0.93 Å. Movie frame rate was fixed at 60 frames per second. Movies were collected with a random defocus range of -0.5 µm to -2.0 µm at a detected dose rate of 30 e−/pixel/second (eps), resulting in a total exposure of around 60 e− / Å2.

Cryo-EM data processing

For the first dataset containing 1 mM GMPPCP, movies were aligned with MotionCor2 (Zheng et al., 2017). The CTF was estimated using CTFFIND4 (Rohou and Grigorieff, 2015) in RELION 3.0. All particles were picked manually, assuring there were no false positives in the dataset. Particles were then sorted into bins by diameter using SPIDER (Frank et al., 1981) scripts and a 2D reference stack. The reference stack was generated by starting with a 2D class average from the particle stack, then pixels were added or removed from the center of the nanotube to respectively increase or decrease the position of the protein decoration to generate 20 bins spanning 43-62 nm in diameter. 15,638 particles from the most populated bins were grouped together for further processing.

For the second dataset (2 mM GMPPCP), movies were aligned MotionCor2 (Zheng et al., 2017). CTF was estimated using CTFFIND4 (Rohou and Grigorieff, 2015) supplemented in cryoSPRAC (Punjani et al., 2017). 1,935 micrographs with CTF fit resolution higher than 8 Å were selected for further processing. From the micrographs, 200 filaments particles were picked manually. They were extracted in a small box size of 686. 2D classification is done with a resolution limit of 15 Å, yielding one class with clear GalCer tube features. This 2D class was selected and used as template for a template-based filament tracer in cryoSPARC on 500 micrographs. 98,140 particles were picked in this manner. Another round of 2D classification with resolution limit of 10 Å, yielded 6 good classes with visible tube features. Another round of template-based filament tracer on all micrographs yielded 143,689 particles (box size 960). They are exported using csparc2star.py in pyem package (https://github.com/asarnow/pyem). Particles were binned by 2 for further processing.

RASTR reconstruction

Particles from both datasets were processed in the same manner unless otherwise specified. Briefly, *psi* angles and shifts were determined using an in-house script first. Then diameters were measured by detecting the membrane signal peaks. Particles in the major peak in diameter distribution histogram were grouped. Random 90 or 270 degrees were assigned as

bioRxiv preprint doi: https://doi.org/10.1101/2024.04.04.588123; this version posted April 4, 2024. The copyright holder for this preprint (which was not certified by peer review) is the author/funder, who has granted bioRxiv a license to display the preprint in perpetuity. It is made available under aCC-BY-NC-ND 4.0 International license.

theta angles. Random 0 to 360 degrees were assigned as *phi* angles. Particles were reconstructed without alignment using RELION 3.0 (Zivanov et al., 2018) to create an initial average map. The initial map was averaged along the z-axis to further remove features and yielded the final azimuthal average map.

To decide the ROI size, a series of sphere masks with different diameters, all located at the center of GalCer tubes, were created. Separately, ROI was masked out from the azimuthal average map using the sphere mask. Projections were acquired from the masked map using relion_project command in RELION 3.0. These projections were subtracted from raw images using RASTR script. 2D classification was performed to determine the best ROI diameter. Then 4 masks with that diameter positioned at random rotational position around the tube membrane were used to create RASTR particles, resulting in 3 times more particles. These particles were treated as single particles for refinement. 3D classifications were performed, using a masked azimuthal average map as initial model, with C1 symmetry and 8 classes using RELION 3.0. After 25 iterations, good classes with good features were picked for further processing.

For the 1 mM GMPPCP dataset, one good class appeared after 25 iterations. 13,215 particles contributing to the best map from 3D classification were further refined in *cis*TEM with a particle-shaped mask. The Euler angle search was constrained to search only *theta* and *phi*, which converged after four iterations. Then all three Euler angles were refined to convergence using local refinement with gradual increases in the search resolution limit in accordance with the FSC. Local refinement was performed with gradually increased resolution limit, starting at 20 Å using 20% particles, then increasing to 15 Å using 50% particles; each went for 5 iterations. A final 10 iterations of local refinement with resolution limit at 10 Å using all particles were performed to get the final Drp1 map. The final map was post-processed in *cis*TEM and low-pass filtered to remove noise.

For 2 mM GMPPCP dataset, using the featureless azimuthal average map as an initial model, none of the 8 classes yielded a map with clear lattice features. The final map obtained from 1 mM GMPPCP dataset was used as initial model, and a non-uniform refinement was performed. The output map (relaxed state map) represented good stalk features at the center rung but smeared out densities away from center. To further investigate the whole dataset, particles were first reimported into RELION and classified in 3D using the relaxed state map as reference. Three classes appeared with lower resolutions but consistent stalk features were observed. Differences appeared in the distance of rung spacing were evident. Further refinement could not improve the resolution or quality of the map. Particles were then imported into cryoDRGN 2.2.0. Particles were first binned to box size 120 for initial training, then binned to box size 240 for more accurate training.

Model building

The starting tetramer model was built using two different dimer models. For the upper dimer, two monomers the crystal structure were aligned to the G domain interface of a GTPase-GED fusion dimer of Dynamin 1 complexed with GMPPCP (PDB ID: 3ZYC). The lower dimer was built using two monomers from the cryo-EM filament structure with an extended BSE (PDB ID: 5WP9), the G domains were aligned in the same manner described above. The VD was modeled using the Drp1 structure predicted by AlphaFold (Jumper et al., 2021; Jumper and Hassabis,

bioRxiv preprint doi: https://doi.org/10.1101/2024.04.04.588123; this version posted April 4, 2024. The copyright holder for this preprint (which was not certified by peer review) is the author/funder, who has granted bioRxiv a license to display the preprint in perpetuity. It is made available under aCC-BY-NC-ND 4.0 International license.

2022). Maintaining the G-G interface, each dimer was fit within the cryo-EM density using rigid body docking in Chimera 1.13 (Pettersen et al., 2004). Four additional chains were docked within the structure to constrain the starting tetramer. In VMD, an all-atom model was generated using the Automatic PSF Builder in VMD28. Files were prepared for NAMD processing following previously described methods (Trabuco et al., 2008). The density map was converted to an MDFF potential. Secondary restraints were applied using NAMD's extrabonds feature and plugins to preserve secondary structure and to limit artifacts to chiral centers and cis peptide bonds. For simulations, the GScale was set to 0.3, the temperature was set to 300, and the number of timesteps (numsteps) was 25,000. A minimization step was run with a GScale was set to 10, temperature was set to 300, and minimize steps (minsteps) was set to 2000. The model was then minimized and refined using Phenix Real-space refinement (Afonine et al., 2018; Liebschner et al., 2019) to fix clashes and outliers.

Sub-particle reconstruction

Coordinates of the alpha carbon in amino acid P499 (the starting of VD) were used to calculate the offset for sub-particle centers. Nine offsets were calculated focusing on the center of the stacked state lattice. Nine sub-particles were extracted from every raw particle with box size 128. To create an initial model, *phi* angle offsets were calculated based on the offsets and added/subtracted directly into metadata. A simple relion_reconstruct yielded the initial map. Sub-particles were refined without imposing symmetry in *cis*TEM suite.

ACKNOWLEDGEMENTS

K.R. discloses support for the research of this work from the National Institute of General Medical Sciences [F31 GM139324]. S.M.S. discloses support for the research and publication of this work from National Institute of General Medical Sciences [R01 GM108753] and [R01 GM143805]. J.A.M. discloses support for the research and publication of this work from National Institute of General Medical Sciences [R01 GM125844].

Molecular graphics images were produced using the UCSF Chimera package from the Resource for Biocomputing, Visualization, and Informatics at the University of California, San Francisco (supported by NIH P41 RR-01081).

AUTHOR CONTRIBUTIONS

Conceptualization: Peng, R., Rochon, K., Stagg, S.M., and Mears, J.A.; Funding acquisition: Rochon, K., Stagg, S.M., and Mears, J.A.; Sample Preparation: Rochon, K. and Mears, J.A.; Imaging and Data Acquisition: Peng, R., Stagg, S.M., and Mears, J.A.; Image Processing Methodology: Peng, R. and Stagg, S.M.; Model building: Rochon, K.; Supervision: Stagg, S.M., and Mears, J.A.; Writing, reviewing and editing: Peng, R., Rochon, K., Stagg, S.M., and Mears, J.A.

bioRxiv preprint doi: https://doi.org/10.1101/2024.04.04.588123; this version posted April 4, 2024. The copyright holder for this preprint (which was not certified by peer review) is the author/funder, who has granted bioRxiv a license to display the preprint in perpetuity. It is made available under aCC-BY-NC-ND 4.0 International license.

REFERENCES

Adachi, Y., M. Iijima, and H. Sesaki. 2018. An unstructured loop that is critical for interactions of the stalk domain of Drp1 with saturated phosphatidic acid. *Small GTPases*. 9:472-479.

Adachi, Y., K. Itoh, T. Yamada, K.L. Cerveny, T.L. Suzuki, P. Macdonald, M.A. Frohman, R. Ramachandran, M. Iijima, and H. Sesaki. 2016. Coincident Phosphatidic Acid Interaction Restrains Drp1 in Mitochondrial Division. *Mol Cell*. 63:1034-1043.

Afonine, P.V., B.K. Poon, R.J. Read, O.V. Sobolev, T.C. Terwilliger, A. Urzhumtsev, and P.D. Adams. 2018. Real-space refinement in PHENIX for cryo-EM and crystallography. *Acta Crystallogr D Struct Biol*. 74:531-544.

Alvarez, F.J.D., S. He, J.R. Perilla, S. Jang, K. Schulten, A.N. Engelman, S.H.W. Scheres, and P. Zhang. 2017. CryoEM structure of MxB reveals a novel oligomerization interface critical for HIV restriction. *Sci Adv*. 3:e1701264.

Bauer, B.L., K. Rochon, J.C. Liu, R. Ramachandran, and J.A. Mears. 2023. Disease-associated mutations in Drp1 have fundamentally different effects on the mitochondrial fission machinery. *Hum Mol Genet*. 32:1975-1987.

Bugge, K., I. Brakti, C.B. Fernandes, J.E. Dreier, J.E. Lundsgaard, J.G. Olsen, K. Skriver, and B.B. Kragelund. 2020. Interactions by Disorder - A Matter of Context. *Front Mol Biosci*. 7:110.

Bustillo-Zabalbeitia, I., S. Montessuit, E. Raemy, G. Basañez, O. Terrones, and J.C. Martinou. 2014. Specific interaction with cardiolipin triggers functional activation of Dynamin-Related Protein 1. *PLoS One*. 9:e102738.

Chappie, J.S., S. Acharya, M. Leonard, S.L. Schmid, and F. Dyda. 2010. G domain dimerization controls dynamin's assembly-stimulated GTPase activity. *Nature*. 465:435-440.

Chappie, J.S., J.A. Mears, S. Fang, M. Leonard, S.L. Schmid, R.A. Milligan, J.E. Hinshaw, and F. Dyda. 2011. A pseudoatomic model of the dynamin polymer identifies a hydrolysis-dependent powerstroke. *Cell*. 147:209-222.

Clinton, R.W., B.L. Bauer, and J.A. Mears. 2020. Affinity Purification and Functional Characterization of Dynamin-Related Protein 1. *Methods Mol Biol*. 2159:41-53.

Clinton, R.W., C.A. Francy, R. Ramachandran, X. Qi, and J.A. Mears. 2016. Dynamin-related Protein 1 Oligomerization in Solution Impairs Functional Interactions with Membrane-anchored Mitochondrial Fission Factor. *The Journal of biological chemistry*. 291:478-492.

Egelman, E.H. 2007. The iterative helical real space reconstruction method: surmounting the problems posed by real polymers. *J Struct Biol*. 157:83-94.

Francy, C.A., F.J. Alvarez, L. Zhou, R. Ramachandran, and J.A. Mears. 2015. The mechanoenzymatic core of dynamin-related protein 1 comprises the minimal machinery required for membrane constriction. *The Journal of biological chemistry*. 290:11692-11703.

Francy, C.A., R.W. Clinton, C. Frohlich, C. Murphy, and J.A. Mears. 2017. Cryo-EM Studies of Drp1 Reveal Cardiolipin Interactions that Activate the Helical Oligomer. *Scientific reports*. 7:3.

Fröhlich, C., S. Grabiger, D. Schwefel, K. Faelber, E. Rosenbaum, J. Mears, O. Rocks, and O. Daumke. 2013. Structural insights into oligomerization and mitochondrial remodelling of dynamin 1 ‐ like protein. *The EMBO Journal*. 32:1280-1292.

Fung, H.Y.J., M. Birol, and E. Rhoades. 2018. IDPs in macromolecular complexes: the roles of multivalent interactions in diverse assemblies. *Curr Opin Struct Biol*. 49:36-43.

bioRxiv preprint doi: https://doi.org/10.1101/2024.04.04.588123; this version posted April 4, 2024. The copyright holder for this preprint (which was not certified by peer review) is the author/funder, who has granted bioRxiv a license to display the preprint in perpetuity. It is made available under aCC-BY-NC-ND 4.0 International license.

Haun, F., T. Nakamura, A.D. Shiu, D.H. Cho, T. Tsunemi, E.A. Holland, A.R. La Spada, and S.A. Lipton. 2013. S-Nitrosylation of Dynamin-Related Protein 1 Mediates Mutant Huntingtin-Induced Mitochondrial Fragmentation and Neuronal Injury in Huntington's Disease. *Antioxidants & Redox Signaling*. 19:1173-1184.

Ingerman, E., E.M. Perkins, M. Marino, J.A. Mears, J.M. McCaffery, J.E. Hinshaw, and J. Nunnari. 2005. Dnm1 forms spirals that are structurally tailored to fit mitochondria. *J Cell Biol*. 170:1021-1027.

Jumper, J., R. Evans, A. Pritzel, T. Green, M. Figurnov, O. Ronneberger, K. Tunyasuvunakool, R. Bates, A. Žídek, A. Potapenko, A. Bridgland, C. Meyer, S.A.A. Kohl, A.J. Ballard, A. Cowie, B. Romera-Paredes, S. Nikolov, R. Jain, J. Adler, T. Back, S. Petersen, D. Reiman, E. Clancy, M. Zielinski, M. Steinegger, M. Pacholska, T. Berghammer, S. Bodenstein, D. Silver, O. Vinyals, A.W. Senior, K. Kavukcuoglu, P. Kohli, and D. Hassabis. 2021. Highly accurate protein structure prediction with AlphaFold. *Nature*. 596:583-589.

Jumper, J., and D. Hassabis. 2022. Protein structure predictions to atomic accuracy with AlphaFold. *Nat Methods*. 19:11-12.

Kalia, R., R.Y. Wang, A. Yusuf, P.V. Thomas, D.A. Agard, J.M. Shaw, and A. Frost. 2018. Structural basis of mitochondrial receptor binding and constriction by DRP1. *Nature*. 558:401-405.

Koirala, S., Q. Guo, R. Kalia, H.T. Bui, D.M. Eckert, A. Frost, and J.M. Shaw. 2013. Interchangeable adaptors regulate mitochondrial dynamin assembly for membrane scission. *Proc Natl Acad Sci U S A*. 110:E1342-1351.

Kong, L., K.A. Sochacki, H. Wang, S. Fang, B. Canagarajah, A.D. Kehr, W.J. Rice, M.P. Strub, J.W. Taraska, and J.E. Hinshaw. 2018. Cryo-EM of the dynamin polymer assembled on lipid membrane. *Nature*. 560:258-262.

Lander, G.C., S.M. Stagg, N.R. Voss, A. Cheng, D. Fellmann, J. Pulokas, C. Yoshioka, C. Irving, A. Mulder, P.W. Lau, D. Lyumkis, C.S. Potter, and B. Carragher. 2009. Appion: an integrated, database-driven pipeline to facilitate EM image processing. *J Struct Biol*. 166:95-102.

Liebschner, D., P.V. Afonine, M.L. Baker, G. Bunkóczi, V.B. Chen, T.I. Croll, B. Hintze, L.W. Hung, S. Jain, A.J. McCoy, N.W. Moriarty, R.D. Oeffner, B.K. Poon, M.G. Prisant, R.J. Read, J.S. Richardson, D.C. Richardson, M.D. Sammito, O.V. Sobolev, D.H. Stockwell, T.C. Terwilliger, A.G. Urzhumtsev, L.L. Videau, C.J. Williams, and P.D. Adams. 2019. Macromolecular structure determination using X-rays, neutrons and electrons: recent developments in Phenix. *Acta Crystallogr D Struct Biol*. 75:861-877.

Liu, J., F.J.D. Alvarez, D.K. Clare, J.K. Noel, and P. Zhang. 2021. CryoEM structure of the super-constricted two-start dynamin 1 filament. *Nat Commun*. 12:5393.

Macdonald, P.J., C.A. Francy, N. Stepanyants, L. Lehman, A. Baglio, J.A. Mears, X. Qi, and R. Ramachandran. 2016. Distinct Splice Variants of Dynamin-related Protein 1 Differentially Utilize Mitochondrial Fission Factor as an Effector of Cooperative GTPase Activity. *J Biol Chem*. 291:493-507.

Macdonald, P.J., N. Stepanyants, N. Mehrotra, J.A. Mears, X. Qi, H. Sesaki, and R. Ramachandran. 2014. A dimeric equilibrium intermediate nucleates Drp1 reassembly on mitochondrial membranes for fission. *Molecular biology of the cell*. 25:1905-1915.

Mahajan, M., N. Bharambe, Y. Shang, B. Lu, A. Mandal, P. Madan Mohan, R. Wang, J.C. Boatz, J. Manuel Martinez Galvez, A.V. Shnyrova, X. Qi, M. Buck, P.C.A. van der Wel, and R.

bioRxiv preprint doi: https://doi.org/10.1101/2024.04.04.588123; this version posted April 4, 2024. The copyright holder for this preprint (which was not certified by peer review) is the author/funder, who has granted bioRxiv a license to display the preprint in perpetuity. It is made available under aCC-BY-NC-ND 4.0 International license.

Ramachandran. 2021. NMR identification of a conserved Drp1 cardiolipin-binding motif essential for stress-induced mitochondrial fission. *Proc Natl Acad Sci U S A*. 118.

Mears, J.A., L.L. Lackner, S. Fang, E. Ingerman, J. Nunnari, and J.E. Hinshaw. 2011. Conformational changes in Dnm1 support a contractile mechanism for mitochondrial fission. *Nat Struct Mol Biol*. 18:20-26.

Nguyen, H.C., N. Talledge, J. McCullough, A. Sharma, F.R. Moss, J.H. Iwasa, M.D. Vershinin, W.I. Sundquist, and A. Frost. 2020. Membrane constriction and thinning by sequential ESCRT-III polymerization. *Nat Struct Mol Biol*. 27:392-399.

Nolden, K.A., J.M. Egner, J.J. Collier, O.M. Russell, C.L. Alston, M.C. Harwig, M.E. Widlansky, S. Sasorith, I.A. Barbosa, A.G. Douglas, J. Baptista, M. Walker, D.E. Donnelly, A.A. Morris, H.J. Tan, M.A. Kurian, K. Gorman, S. Mordekar, C. Deshpande, R. Samanta, R. McFarland, R.B. Hill, R.W. Taylor, and M. Oláhová. 2022. Novel DNM1L variants impair mitochondrial dynamics through divergent mechanisms. *Life Sci Alliance*. 5.

Nunnari, J., and A. Suomalainen. 2012. Mitochondria: in sickness and in health. *Cell*. 148:1145-1159.

Osellame, L.D., A.P. Singh, D.A. Stroud, C.S. Palmer, D. Stojanovski, R. Ramachandran, and M.T. Ryan. 2016. Cooperative and independent roles of the Drp1 adaptors Mff, MiD49 and MiD51 in mitochondrial fission. *J Cell Sci*. 129:2170-2181.

Otera, H., N. Ishihara, and K. Mihara. 2013. New insights into the function and regulation of mitochondrial fission. *Biochim Biophys Acta*. 1833:1256-1268.

Peng, R., X. Fu, J.H. Mendez, P.S. Randolph, B.E. Bammes, and S.M. Stagg. 2023. Characterizing the resolution and throughput of the Apollo direct electron detector. *J Struct Biol X*. 7:100080.

Pettersen, E.F., T.D. Goddard, C.C. Huang, G.S. Couch, D.M. Greenblatt, E.C. Meng, and T.E. Ferrin. 2004. UCSF Chimera--a visualization system for exploratory research and analysis. *J Comput Chem*. 25:1605-1612.

Punjani, A., J.L. Rubinstein, D.J. Fleet, and M.A. Brubaker. 2017. cryoSPARC: algorithms for rapid unsupervised cryo-EM structure determination. *Nat Methods*. 14:290-296.

Randolph, P.S., and S.M. Stagg. 2020. Reconstruction of Average Subtracted Tubular Regions (RASTR) enables structure determination of tubular filaments by cryo-EM. *J Struct Biol X*. 4:100023.

Reubold, T.F., K. Faelber, N. Plattner, Y. Posor, K. Ketel, U. Curth, J. Schlegel, R. Anand, D.J. Manstein, F. Noé, V. Haucke, O. Daumke, and S. Eschenburg. 2015. Crystal structure of the dynamin tetramer. *Nature*. 525:404-408.

Robertson, G.L., S. Riffle, M. Patel, C. Bodnya, A. Marshall, H.K. Beasley, E. Garza-Lopez, J. Shao, Z. Vue, A. Hinton, M.S. Stoll, S. de Wet, R.P. Theart, R.P. Chakrabarty, B. Loos, N.S. Chandel, J.A. Mears, and V. Gama. 2023. DRP1 mutations associated with EMPF1 encephalopathy alter mitochondrial membrane potential and metabolic programs. *J Cell Sci*. 136.

Rochon, K., B.L. Bauer, N.A. Roethler, Y. Buckley, C.C. Su, W. Huang, R. Ramachandran, M.S.K. Stoll, E.W. Yu, D.J. Taylor, and J.A. Mears. 2024. Structural basis for regulated assembly of the mitochondrial fission GTPase Drp1. *Nat Commun*. 15:1328.

Rohou, A., and N. Grigorieff. 2015. CTFFIND4: Fast and accurate defocus estimation from electron micrographs. *J Struct Biol*. 192:216-221.

bioRxiv preprint doi: https://doi.org/10.1101/2024.04.04.588123; this version posted April 4, 2024. The copyright holder for this preprint (which was not certified by peer review) is the author/funder, who has granted bioRxiv a license to display the preprint in perpetuity. It is made available under aCC-BY-NC-ND 4.0 International license.

Suloway, C., J. Pulokas, D. Fellmann, A. Cheng, F. Guerra, J. Quispe, S. Stagg, C.S. Potter, and B. Carragher. 2005. Automated molecular microscopy: the new Leginon system. *J Struct Biol*. 151:41-60.

Sundborger, A.C., S. Fang, J.A. Heymann, P. Ray, J.S. Chappie, and J.E. Hinshaw. 2014. A dynamin mutant defines a superconstricted prefission state. *Cell Rep*. 8:734-742.

Sweitzer, S.M., and J.E. Hinshaw. 1998. Dynamin undergoes a GTP-dependent conformational change causing vesiculation. *Cell*. 93:1021-1029.

Trabuco, L.G., E. Villa, K. Mitra, J. Frank, and K. Schulten. 2008. Flexible fitting of atomic structures into electron microscopy maps using molecular dynamics. *Structure*. 16:673-683.

Ugarte-Uribe, B., H.M. Müller, M. Otsuki, W. Nickel, and A.J. García-Sáez. 2014. Dynamin-related protein 1 (Drp1) promotes structural intermediates of membrane division. *J Biol Chem*. 289:30645-30656.

von der Malsburg, A., G.M. Sapp, K.E. Zuccaro, A. von Appen, F.R. Moss, R. Kalia, J.A. Bennett, L.A. Abriata, M. Dal Peraro, M. van der Laan, A. Frost, and H. Aydin. 2023. Structural mechanism of mitochondrial membrane remodelling by human OPA1. *Nature*. 620:1101-1108.

Wang, H., P. Song, L. Du, W. Tian, W. Yue, M. Liu, D. Li, B. Wang, Y. Zhu, C. Cao, J. Zhou, and Q. Chen. 2011. Parkin ubiquitinates Drp1 for proteasome-dependent degradation: implication of dysregulated mitochondrial dynamics in Parkinson disease. *J Biol Chem*. 286:11649-11658.

Warnock, D.E., J.E. Hinshaw, and S.L. Schmid. 1996. Dynamin self-assembly stimulates its GTPase activity. *J Biol Chem*. 271:22310-22314.

Wasiak, S., R. Zunino, and H.M. McBride. 2007. Bax/Bak promote sumoylation of DRP1 and its stable association with mitochondria during apoptotic cell death. *J Cell Biol*. 177:439-450.

Wilson-Kubalek, E.M., R.E. Brown, H. Celia, and R.A. Milligan. 1998. Lipid nanotubes as substrates for helical crystallization of macromolecules. *Proc Natl Acad Sci U S A*. 95:8040-8045.

Yan, J., X.H. Liu, M.Z. Han, Y.M. Wang, X.L. Sun, N. Yu, T. Li, B. Su, and Z.Y. Chen. 2015. Blockage of GSK3β-mediated Drp1 phosphorylation provides neuroprotection in neuronal and mouse models of Alzheimer's disease. *Neurobiol Aging*. 36:211-227.

Zhang, P., and J.E. Hinshaw. 2001. Three-dimensional reconstruction of dynamin in the constricted state. *Nat Cell Biol*. 3:922-926.

Zheng, S.Q., E. Palovcak, J.P. Armache, K.A. Verba, Y. Cheng, and D.A. Agard. 2017. MotionCor2: anisotropic correction of beam-induced motion for improved cryo-electron microscopy. *Nat Methods*. 14:331-332.

Zhong, E.D., T. Bepler, B. Berger, and J.H. Davis. 2021. CryoDRGN: reconstruction of heterogeneous cryo-EM structures using neural networks. *Nat Methods*. 18:176-185.

Zivanov, J., T. Nakane, B.O. Forsberg, D. Kimanius, W.J. Hagen, E. Lindahl, and S.H. Scheres. 2018. New tools for automated high-resolution cryo-EM structure determination in RELION-3. *Elife*. 7.